SPACE TELESCOPE
European Coordinating Facility

ST-ECF Instrument Science Report NGST 2002-04

Slit throughput and image quality of a MEMS-type spectrograph for NGST

Wolfram Freudling

Slit throughput and image quality of a MEMS-type spectrograph for NGST

W. Freudling (ST-ECF)

V1.1 September 2002

Abstract
The slits of the NIRSpec spectrograph currently designed for NGST will probably be formed by arrays of micro-electromechanical system (MEMS). Initially, both mirrors and shutters were considered for the optical elements of these arrays. Recently, however, the decision was taken not to further pursue the mirror option. In this report, we evaluate the optical performance of both kinds of system. The investigation is carried out using a simple Fourier model of an optical system consisting of a telescope with attached spectrograph. It is used to evaluate the effects of diffraction on a slit comprising a small array of individual MEMS facets. Throughput and contrast are computed for a range of parameters and comparisons are made of the performance of different technological solutions.

1. Introduction

The preferred slit-generating system for the Next Generation Space Telescope Near-Infrared Spectrograph (NIRSpec) is an array of micro shutters or mirrors. The individual elements of such a micro electromechanical system (MEMS), called facets, can be individually commanded to block light or direct it toward the collimator of the spectrograph. Several facets will be turned 'ON' to form an effective slit. The size of the facets on the sky will be chosen so that the desired slit widths can be achieved by opening two or more adjacent facets. The advantage of such a system is the flexibility with which slit can be placed at virtually any position in the focal plane. However, diffraction due to the gaps between facets and possible phase shifts will reduce the throughput of such slits. In this study, we use a Fourier analysis of a basic telescope-spectrograph combination to explore the nature of these effects and estimate the total efficiency of such a spectrograph.

2. Optical Configuration

2.1 Light path

The model we used in this study includes only the essential optical elements which are shown in figure 1. Incoming light passes through the telescope aperture A and is projected onto the slit S. The telescope is fully specified by its entrance pupil, the focal ratio $f_t = 1/18$ and its aberration (see below). The diameter of the entrance pupil was taken to be 6.25 m. Two different entrance pupils were considered. One is a simple circular aperture with a circular central aperture of 15%. Alternatively, the entrance pupil was assumed to consist of a segmented mirror with a support structure as shown in figure~2. This aperture is not meant

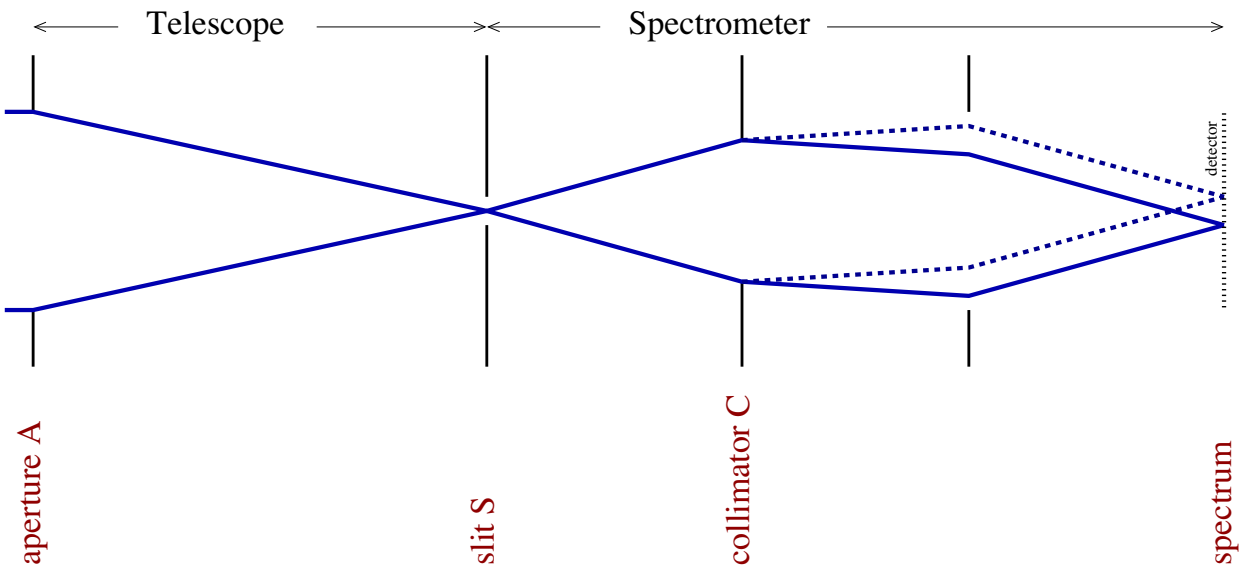

Figure 1: *Schematic optical path of the Fourier model. The planes labeled in red (vertical type) are alternating pupils and focal planes. The assumed aperture at plane A is the input for the model. The incoming beam at each of the subsequent planes is computed from a Fourier transform of the previous plane.*

to represent any current NGST design but rather serves as an example of a complex pupil function. The aperture was kindly provided by J. Krist.

The telescope was assumed to add some phase errors to the incoming beam. These phase errors are described by Zernike polynomials. Regardless of the aperture used, Zernike polynomials which are orthogonal within a circular aperture with a central obscuration of 20% were used. The magnitude of the aberration terms are chosen so that the rms wavefront error within the aperture is 0.1μm for the segmented mirror. The values used for each polynomial are given in table 1. Since a circular mirror without any obscuration from the support structure is overly optimistic, the aberration terms were in this case deliberately chosen to be somewhat pessimistic. For that reason, the terms given in the table 1 were doubled, leading to an rms wavefront error of about 0.2μm.

The slit was assumed to consist of 6 individual facets with a projected size on the sky of 100 × 200 mas each (figure 3). The facets are separated by a gap. These gaps were assumed to be completely 'black', i.e. they absorb all incoming light. The size of the gap is specified by the filling factor of the facets. The facets that form a slit can be chosen so that the location of the PSF is always within half a facet of the center. If shutters are used to generate the slits, diffraction on the grid formed by the shutters will spread the beam which reaches the

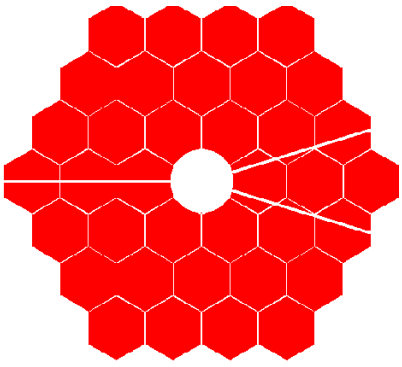

Figure 2: *Assumed entrance pupil of telescope. The primary telescope mirror is assumed to consist of hexagonal elements. The projected size of the secondary mirror is 15% of the telescope diameter. Some arbitrary support structure is shown.*

spectrograph aperture. Therefore, some light will be lost there. The fraction of light lost at the entrance pupil of the spectrograph depends on its size. If the facets are made of mirrors, the same effect occurs but additional phase errors will be introduced by the slit. This is because each mirror is located close to but not exactly at the focal plane (see figure 4). Let Δy be the distance between the focal plane and the facet location. The thickness of the layer defined by the facet, i.e. the maximum of Δy was assumed to be 0.2μm. In addition, each mirror was allowed to tilt in any direction up to a tilt angle α of 0.1°. This assumed that tilt errors are small relative to the beam size and therefore their effect on both the PSF and efficiency is expected to be small.

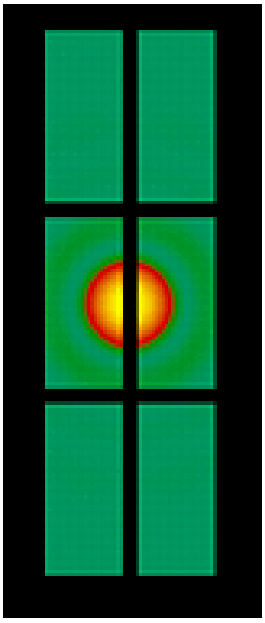

Figure 3: *Shape of slit formed by 6 facets. This is the standard slit configuration used for wavelengths shorter than 3μm. Superimposed is the PSF computed from the segmented mirror for a wavelength of 1.6μm.*

The spectrograph itself consists of a collimator with entrance aperture *C* and a disperser. Different sizes for this aperture have been considered. These sizes are specified relative to the size corresponding to the situation when the focal ratio of the telescope is identical to the that of the spectrograph.

2.2 Model parameters

Most results in section 4 are first discussed for $\lambda = 1.6\mu m$, which serves as a reference wavelengths. Tables 1 and 2 summarise the parameters used for the telescope and MEMS. Unless otherwise noted, these parameters were employed in the discussion below.

3. Fourier model

3.1 Formalism

One purpose of this study is to demonstrate the effect of generating the slit with several facets of a MEMS device, which are separated by gaps, on the total throughput and PSF of a spectrograph. In the case of mirrors, phase shifts will be imposed on incoming wave fronts. It can therefore easily be included in a Fourier approximation of the spectrograph. The results of a Fourier analysis should be useful to identify the major effects. Such an analysis is presented here.

The basic design of our model is shown in figure 1. In a Fourier approximation, the

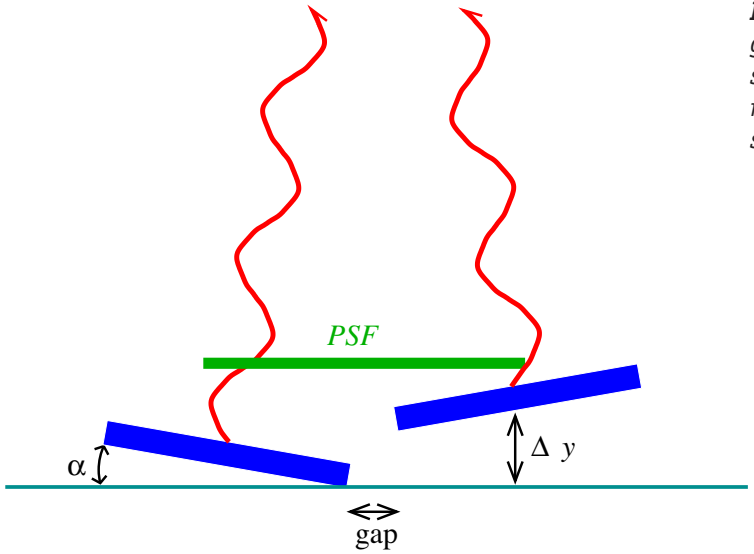

Figure 4: *Cross-section through slit generating mirrors. The mirror elements are shown in blue. The red waves indicate the reflected light, the incoming light is not shown. This cartoon is not drawn to scale.*

Table 1: *Telescope parameters*

	Parameter	Assumed value
Aperture		
	shape	circular or segmented
	diameter	6.25m
	central obscuration	15%
	focal ratio	$f/18$
Aberration[1]		
	focus	0.0
	x coma	0.01
	y coma	-0.01
	0° astigmatism	0.005
	45° astigmatism	-0.005
	spherical	0.15
	resulting rms wavefront errors	0.1μm
Spectrograph		
	focal ratio	$f/15$ = 20% oversizing
	size of detector pixel	0.064 arcsec
	dispersion	0.05μm per pixel
	slit size λ < 3μm	0.2 × 0.6 arcsec
	slit size λ > 3μm	0.3 × 0.6 arcsec

[1] *twice these values were used for the circular aperture*

Table 2: *MEMS parameters*

parameter	unit	assumed value for micro shutters	assumed value for micro mirrors
size of facets	arcsec2	0.1 × 0.2	0.1 × 0.2
filling factor	%	68	92
max phase shift (piston)	μm	0	0.8
max tilt error	degree	0	0.1
tilt in OFF state	degree	n/a	10

wavefront can be mapped from the pupil to the focal plane and vice versa with a simple Fourier transform $\mathcal{F}$. Following the path of figure 1, this is done in the following steps.

- The field $\mathbf{U}_i$ at aperture A is closely approximated by a plane wave. Assumed aberrations of the telescope are included as deviations from a plane wave front. If A is the a function which is unity within the aperture shown in figure 2 and zero outside, $\mathbf{U}_i$ can be written as

$$\mathbf{U}_i = A\, e^{i\phi(x,y)} \tag{1}$$

  where $e^{i\phi(x,y)}$ are the phases due to aberration. The phase errors ϕ were approximated with Zernike polynomials with some arbitrarily assumed coma, astigmatism and spherical aberration. The assumed values are given in table 1. The total rms wavefront error is 0.1μm.

- Just before slit, the field $\mathbf{U}_p$ can then be computed as

$$\mathbf{U}_p = \mathcal{F}(\mathbf{U}_i) \tag{2}$$

- At the slit, the phase errors are added:

$$\mathbf{U}_s = \mathbf{U}_p \,.\, \mathbf{S} = \mathcal{F}(\mathbf{U}_i) \,.\, \mathbf{S} \tag{3}$$

  The slit S is $\mathbf{S} = S_0\, e^{i\theta(x,y)}$, where $e^{i\theta(x,y)}$ is the phase added by the MEMS. These phases include the a component due to the offsets of the mirrors, $\theta = 2\pi\, \Delta y/\lambda$. In addition, the tilt of the mirror is added which changes the phase as a function of position on the mirror. For micro-shutters,

$$S_0 = \begin{cases} 1 & \text{if MEMS on} \\ 0 & \text{if MEMS off} \end{cases} \tag{4}$$

  whereas for micro-mirrors, $\mathbf{S} = S_0\, e^{i\theta(x,y)}$,

$$S_0 = \begin{cases} 1 & \text{if MEMS on} \\ e^{\theta(x,y)} & \text{if MEMS off} \end{cases} \tag{5}$$

  where θ is a phase shift which corresponds to a 10° tilt ot the mirror.

- The collimator entry aperture is again described by a function C which is unity where the stop is transparent and zero otherwise:

$$\mathbf{U}_c = \mathcal{F}(\mathbf{U}_s) \,.\, \mathbf{C} \tag{6}$$

  where $C = \text{abs}(\mathbf{C}) = \begin{cases} 1 & \text{within stop} \\ 0 & \text{else} \end{cases}$

- In section 6.2, additional wavefront errors are added in plane C to similate the performance of the spectrograph optics after the slit. These are included in function $\mathbf{C}$ as

$$\mathbf{C} = C \,.\, \exp(\theta_s(x,y)) \tag{7}$$

- Finally, the spectrum of a monochromatic point source can be computed:

$$\mathbf{U}_s = \mathcal{F}(\mathbf{U}_c) \tag{8}$$

3.2 Implementation

The most critical numerical consideration is the projection of the different optical elements onto an array with sufficiently accurate spatial sampling while simultaneously requiring reasonable CPU times for the necessary FFTs. The model was implemented in IDL. Array sizes of n × n = 1024 × 1024 were used for most runs, and n × n = 2048 × 2048 arrays were used

for selected models to test whether the smaller array contained a sufficiently large fraction of the flux to support the conclusions.

The size of the telescope aperture has to be selected so that both the aperture plane and the PSF in the imaging plane are sufficiently sampled. Nyquist sampling is achieved by choosing the diameter of the telescope aperture to be half the array size. The scale per pixel in the slit plane is then

$$\delta = 1/2 \,.\, \lambda_c/D \,.\, (360 \,.\, 3600''/2\pi), \qquad (9)$$

where λ_c is the wavelength with Nyquist sampling. This specifies the scale of the facets in pixels. In most cases, the scale of the facets in array pixels was chosen to be 50 pixels, and λ_c was chosen to be $1/10^{th}$ of the shortest considered wavelength. This choice determines the telescope diameter D. The size of the collimator aperture D_c without oversizing is the same as the telescope aperture size. If $o = f_s/f_t$ is the oversizing, then

$$D_c = o \,.\, D \qquad (10)$$

The angular diameter of the collimator aperture as seen from the slit d_c is given by $\sin(d_c) = f_s$. This specifies the relation between phase shifts at the slits and tilt of the mirrors. A tilt α is implemented as a phase shift $p = \sin(\alpha)\, f_s/4$. This phase shift is imposed on the beam by multiplying the field U_s in equation 3 with

$$e^{i\phi(x,y)} = A\, e^{-2i\pi p(x_r - n/2)/(f_s \,.\, n/4)} \qquad (1)$$

where x_r is the pixel coordinate relative to the center of the mirror rotated by the direction of the tilt.

4. Spectrograph efficiency

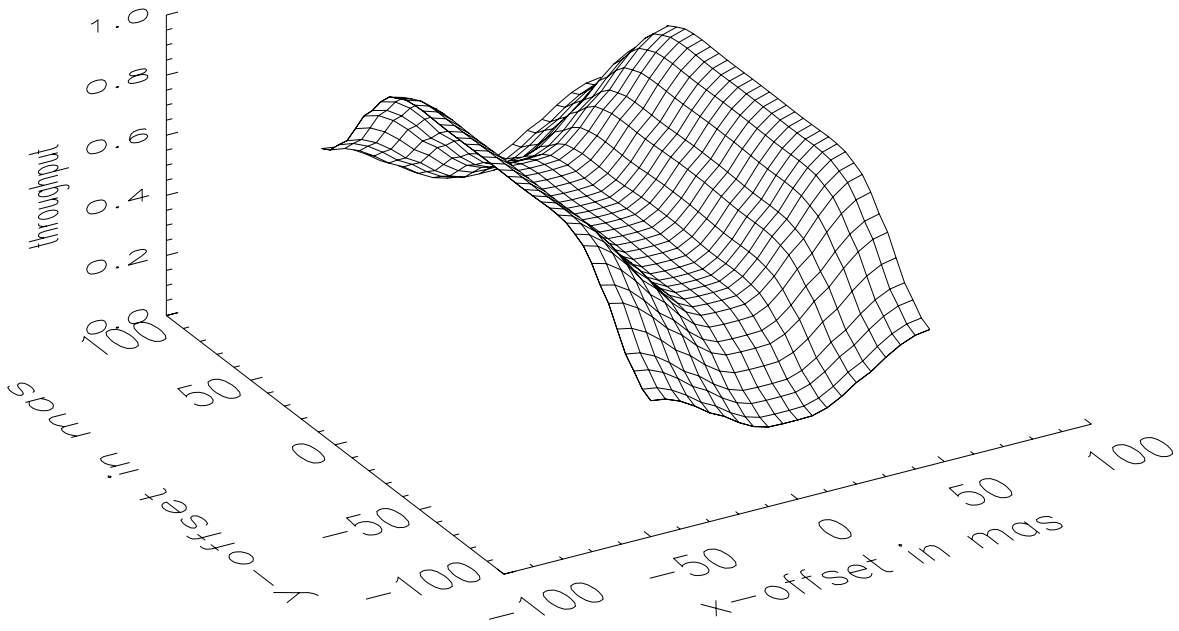

Figure 5: Efficiency of a micro-shutter generated slit as a function of dither position assuming the circular telescope entrance pupil at λ =1.6μm. X-offset and Y-offset are zero when the PSF is centered in the slit as shown in figure 3.

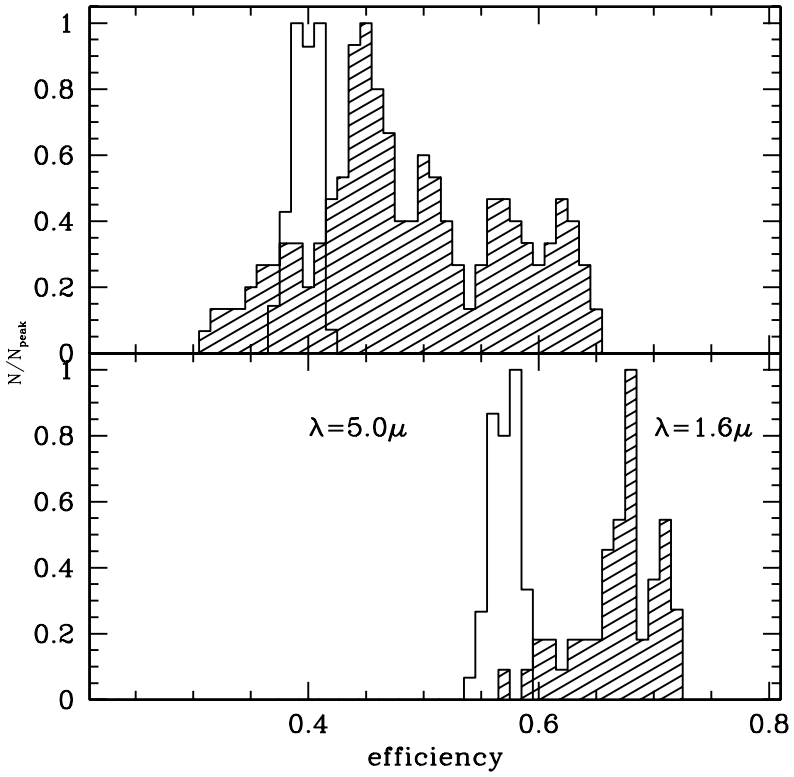

Figure 6: *Distribution of MEMS efficiencies for different dither positions. Histograms for λ=1.6μm and λ=5.0μm. The upper panel shows the distribution for micro-shutters and the lower panel for micro-mirrors. A 2 × 3 facet slit was used for 1.6μm and 3 × 3 slit for 5.0μm. The telescope aperture in all cases was assumed to be the segmented mirror.*

4.1 Efficiency variations with dither position

The total throughput of the telescope and spectrograph depends on the positions of the PSF within the slit. A single object can be centered in the slit by appropriate pointing of the telescope. To observe additional sources in the fields, facets will be turned 'on' to create slits centered on each object. This centering can be done in steps of half the size of the facets. Objects located more than half the size of a facet from the center of the slit can be avoided by opening a different set of facets.

Two effects modulate the throughput as a function of position within the slit. One effect is the geometrical effect that the part of the PSF which falls into the gap between two facets is lost. In addition, the grid-like shape of the slit will create diffraction in addition to the normal diffraction pattern of a slit. Some of the light which leaves the slit will therefore not reach the aperture of the spectrograph. The amount of light lost at the spectrograph aperture depends on its size, the wavelength and the assumed PSF. In figure 5, the shutter throughput as a function of offset position is shown for the PSF resulting from the circular telescope aperture at a wavelength of 1.6μm. The shape of the slit is the one shown in figure 3. For computational efficiency, only positive offsets were computed and the numbers replicated for negative offsets. The shape of this curve can easily be understood. In the center of the slit, the peak of the PSF falls onto the gap between two facets. As the PSF moves in the *y*-direction away from the center, the total throughput drops sharply as soon as the PSF gets close to a location exactly between four facets. On the other hand, if the PSF is moved from the center along the *x*-axis, the throughput actually increases as the PSF becomes centered within a single facet.

The strong variations in throughput with slit position introduce a significant uncertainty for absolute spectrophotometry. This can be alleviated by repeated exposures which are dithered so that exposures are obtained which place every object at different positions within its slit. Two criteria can be used to evaluate such a strategy. One is the mean

throughput averaged over random dither positions. The second one is the variations of the throughput with dither position. In figure 6, the distribution of throughputs for a dither pattern of 10 × 20 points is shown for two different wavelengths, $\lambda = 1.6\mu m$ and $5.0\mu m$. For the $\lambda = 5.0\mu m$ case, a slit size of 3 × 3 facets was used. The upper panel shows the distribution for micro-shutters. For the longer wavelengths, the mean throughput is smaller because for the larger PSF more light is lost despite the larger slit width. However, the variation of the throughput over the whole dither pattern is smaller since the size of the gaps between facets is small compared to the size of the PSF. Therefore, while the total throughput is smaller for the longer wavelengths, the spectrophotometric uncertainties due to the uncertainty in the position of an object within the slit are smaller. The lower panel of figure 6 shows the same distribution for the mirrors. It can be seen that for each wavelength, the total throughput is larger than for the shutters. This is due to the assumed smaller gaps between the facets, which more than compensates the larger diffraction losses due to the phase shifts introduced by the mirror.

4.2 Efficiency as a function of aperture stop size

The relatively small mean efficiencies and large variations in the throughput of the slits raises the question of whether the assumed 20% oversizing of the spectrograph aperture should be increased. For that purpose, the efficiency of the spectrograph was computed as a function of the aperture size and compared to that of an ideal slit. Figure 7 shows the fraction of light at the spectrograph aperture which passes the aperture stop as a function of the diameter of the aperture. The diameter d_a is given in units of aperture size when the f-number of the spectrograph matches that of the telescope. Below, we will refer to apertures larger than 1 as 'oversized', and use the expression 'oversizing' for $d_a - 1$ expressed as a percentage. Also included are curves for an ideal slit with the same size as the MEMS slit but fully transparent without any gap (green curves). It can be seen that for such an ideal case, 20% oversizing is sufficient to collect virtually all the light which leaves the slit. For the MEMS slit, the loss of light due to the diffraction on the gaps between the facets strongly depends on the dither position (red curves). The mean loss over all dither positions is about 20% with an oversizing of 20%. Larger oversizing leads to smaller losses. However, the gain grows only slowly as a function of oversizing. Figure 8 shows the same curves for different PSF, different wavelengths and different gap sizes. It can be seen that in all considered cases, the gain in efficiency as a function of oversizing grows only slowly once an oversizing of 20% is reached. In all cases, an increase of throughput of 5% over the one with an oversizing of 20% would require an oversizing of at least 70%. This corresponds to an increase in the mirror area of $(1.7/1.2)^2 \sim 2$ which is probably too high a price to pay for the small gain in throughput.

4.3 Efficiency as a function of wavelength

In previous sections, we have used slits which are 3 facets (i.e. 0.3 arcsec) wide for the wavelengths longer than $3\mu m$, while for short wavelengths we used slits only 0.2 arcsec wide. In this section, we investigate the efficiency at different wavelengths with both slit widths to see whether these choices were justified. The upper panel of figure 9 shows the efficiency for both slit widths, both for the mirrors and shutters. The lower panel shows the ratios of the efficiencies of the different slit widths. It can be seen that that the wider slits lead to a noticeably larger throughput at each wavelength. However, the gain from the larger slit width starts to increase significantly at $\lambda \sim 3\mu m$. These results suggests that the use of the wider slits should be kept as an option for the longer wavelengths, where the degradation of

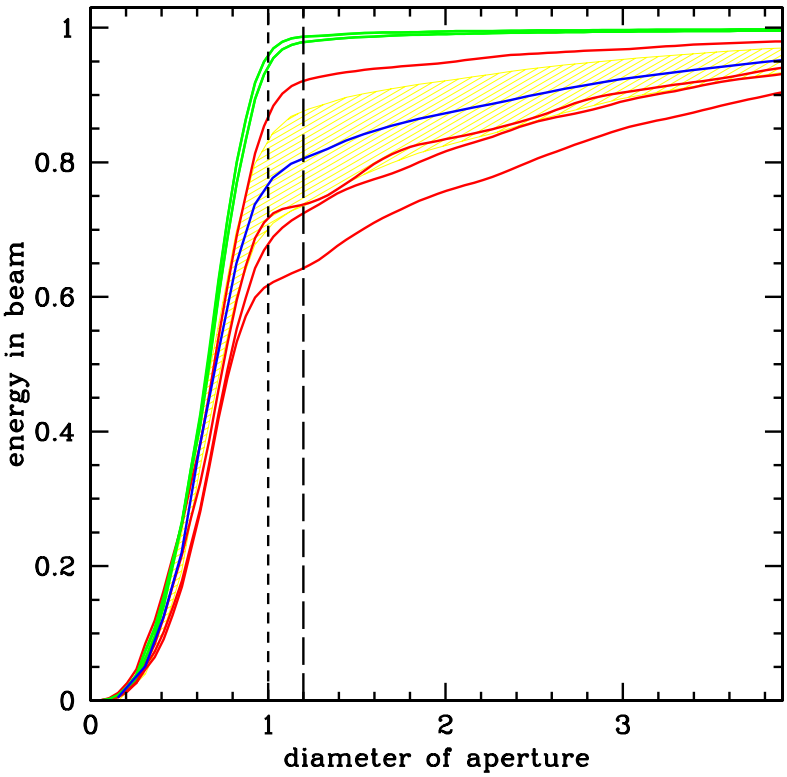

Figure 7: *Aperture efficiency for micro-shutters as a function of the size of the entrance aperture of the spectrograph for λ = 1.6μm. The red curves are the results for the 4 most extreme dither positions. The blue curve is the mean of all dither positions, and the yellow shaded area around the blue curve shows the rms over all dither positions at each diameter. The green curves are the same computations carried out with an ideal, fully transparent slit. The long-dashed line indicates the standard assumption of 20% oversizing.*

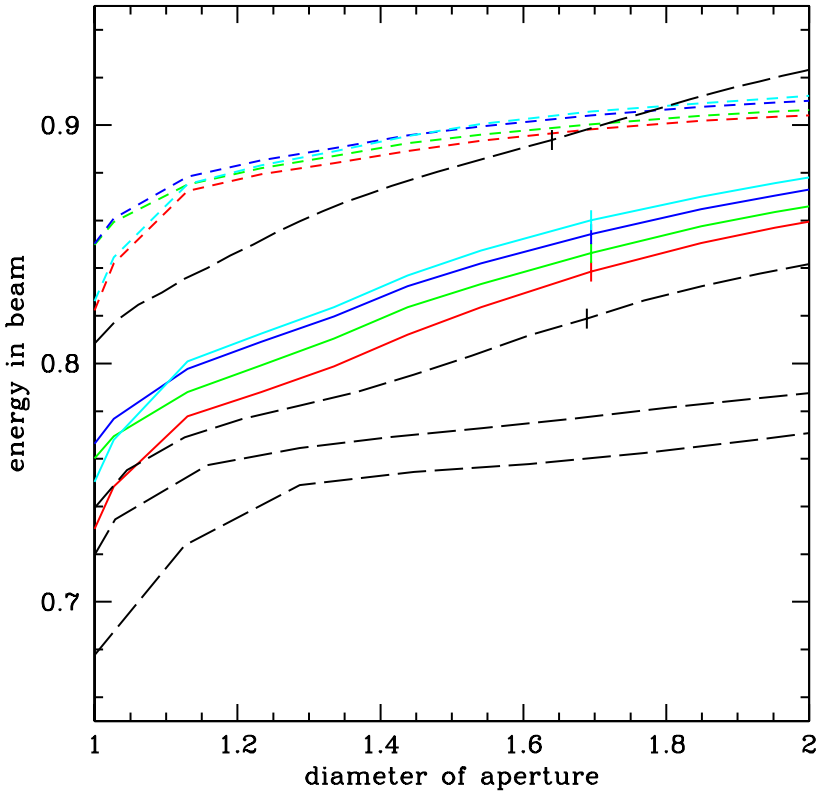

Figure 8: *Efficiency of shutters as a function of the size of the entrance aperture. The solid lines have been computed for two different telescope apertures discussed in the text, once with aberration and once without aberration. The short-dashed lines are the same models but with a gap size between facets reduced to half the nominal size. The long-dashed lines are computed for the standard parameters at λ = 1.6μm, 2.5μm, 4.0μm and 5.0μm. For λ = 4.0μm and 5.0μm, a slit consisting of 3 × 3 facets was used. The points where the efficiency is 5% above the efficiency at a beam size of 1.2 are marked with a dash. For curves without a dash, this point is outside the limits of the plot.*

the spectral resolution is small.

5 Contrast for mirrors

For micro mirrors, a facet can be turned 'OFF' by tilting the micro mirrors. A major concern is the light which will be reflected into the spectrograph aperture by the gaps between the facets. Since the MEMS are in an image plane, this reflected light will produce faint spectra

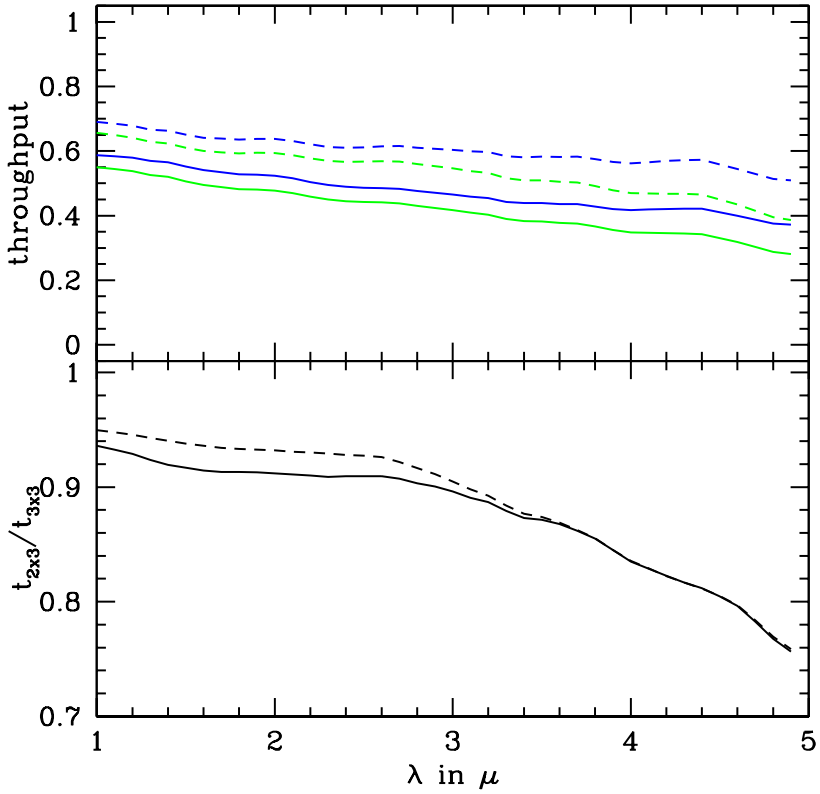

Figure 9: *Upper panel: Efficiency as a function of wavelength for 2 × 3 facets slits (blue), 3 × 3 facets slits (green), both for mirrors (dashed lines) and shutters (solid lines). Lower panel: Ratio of efficiencies for 2 × 3 facets slits to 3 × 3 facets slits. Again, the dashed line is for mirrors, and the solid line for shutters.*

of bright objects even if the MEMS are turned off. One important specification of a mirror array is its ability to suppress such reflection. Even if no reflection on the gaps occurs, the diffraction of light from bright objects on the mirrors arrays will cause some of its light to leak into the spectrograph when the micro mirrors are in the OFF state. The amount of leaked light collected by the spectrograph depends on the size of its aperture. This effect can easily be simulated by our Fourier model. We have computed the intensity of a point-like object with the mirrors of the slit in the ON and OFF states. The contrast, which is defined as the ratio of the two, is plotted for a number of wavelengths as a function of the entrance aperture of the spectrograph in figure 10. These numbers can be considered as the maximum achievable contrast ratio for a given PSF. Because the wings of the PSF determine the intensity in the OFF state, these results are more sensitive to PSF properties than the ones presented in the previous sections. In particular at the shortest wavelengths, the PSF in use might be unrealistic sharp and therefore the achievable contrast might be underestimated. Nevertheless, it can be seen that the achievable contrasts are close to the minimum acceptable, which is about 1000 (Freudling et al., 2002).

6. Image quality at the detector

6.1 Image quality for different positions within MEMS slit

Diffraction at the gaps between the facets not only lowers the total throughput, but in addition degrades the PSF at the detector. The consequence of this degradation is that the spectrum will be smeared, both in wavelength and in the spatial direction. The former will lower the achievable resolution, whereas the latter leads to a lower signal to noise ratio in extracted spectra.

To illustrate this effect, we have simulated observed spectrum images by computing PSF at each wavelength, and adding the normalised PSF after shifting according to an assumed

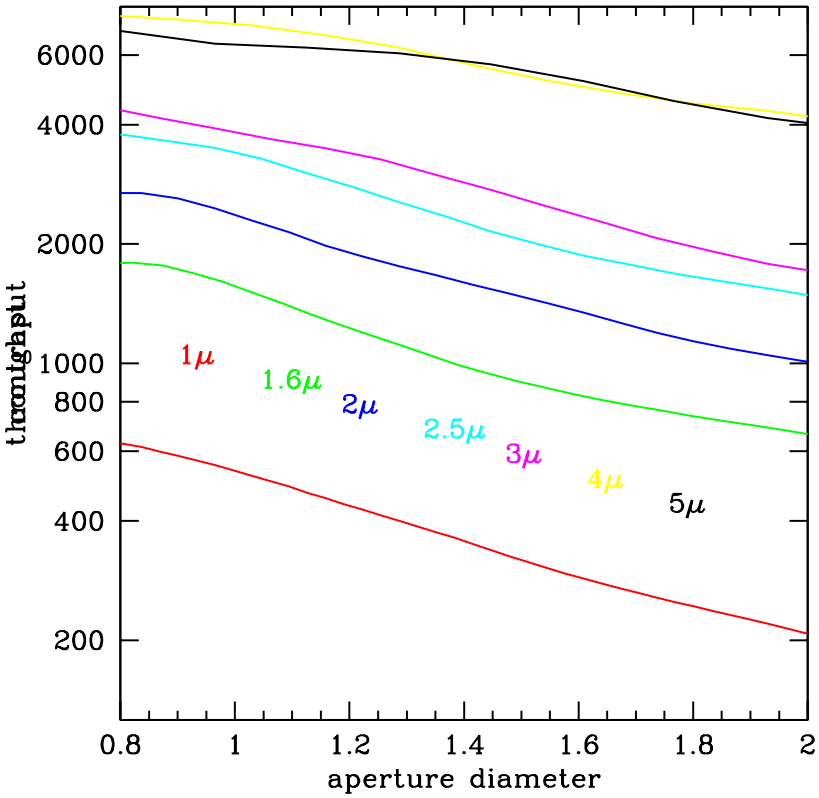

Figure 10: *Contrast for micro-mirror generated slits as a function of the size of the entrance aperture. The different curves are for the wavelengths as indicated in the plot.*

dispersion of 0.05μm/pix. In figure 11, we compare an observed spectral line of an object located in the center of a 2 × 3 slit with that of an object located at the intersection of gaps between facets. Visual comparison of the two spectra already suggests that the PSF quality needs further attention.The image quality for micro-mirror is shown as a single example in figure 12. The impact of phase shifts between facets covered by the PSF at the slit position can easily be recognized. Such effects will strongly depend on mirror properties and are not explored further here.

6.2 Optical fidelity of telescope versus spectrograph

Both the telescope itself and the spectrograph independently introduce wavefront errors, hereafter WFE. In order to explore the impact of these WFE on the image quality, we have modified our model as follows. Until now, all the WFE were assigned to the telescope mirrors. Additional WFE will be introduced in the spectrograph, both in the foreoptics and in the spectrograph proper. The effect of WFE in the foreoptics is the same as WFE in the telescope itself. They can simply be included in the parametrisation of the telescope WFE. The WFE of the optics after the slit can be introduced at plane *C* in figure 1 by modifying equation (7). Hereafter, we will use the terms 'WFE of the telescope' and 'WFE of the spectrograph' to distinguish between the origin of the WFE. Jakobsen (2002) gives one example how the total WFE of 0.180μm could be distributed. In his model, the total WFE for the telescope is 0.158μm, and that of the spectrograph proper is 0.088μm. Below, we explore the performance of such a telescope–spectrograph system by computing monochromatic PSF. The WFE of the spectrograph were taken to be due to spherical aberration.

In a near-perfect imaging system, the Strehl ratio *S* of the resulting PSF only depend on the total WFE introduced by the optics. A simple formula describes this relation (eg. Schroeder, 1987 eq. 10.2.6):

$$S = \exp(-(k \cdot WFE)^2) \qquad (12)$$

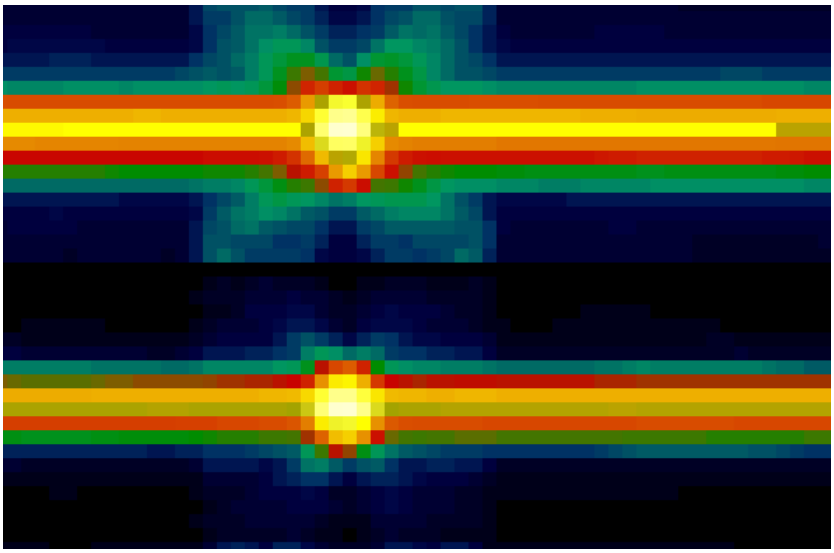

Figure 11: *Simulated line spectra at λ =1.6μm from micro-shutter generated slits. The upper panel is for an object located at the intersection of the gaps, whereas the lower panel is for an object centered in the slit. The color scale is logarithmic. The simulated pixel size is 20 mas, i.e. much smaller than expected size of detector pixels.*

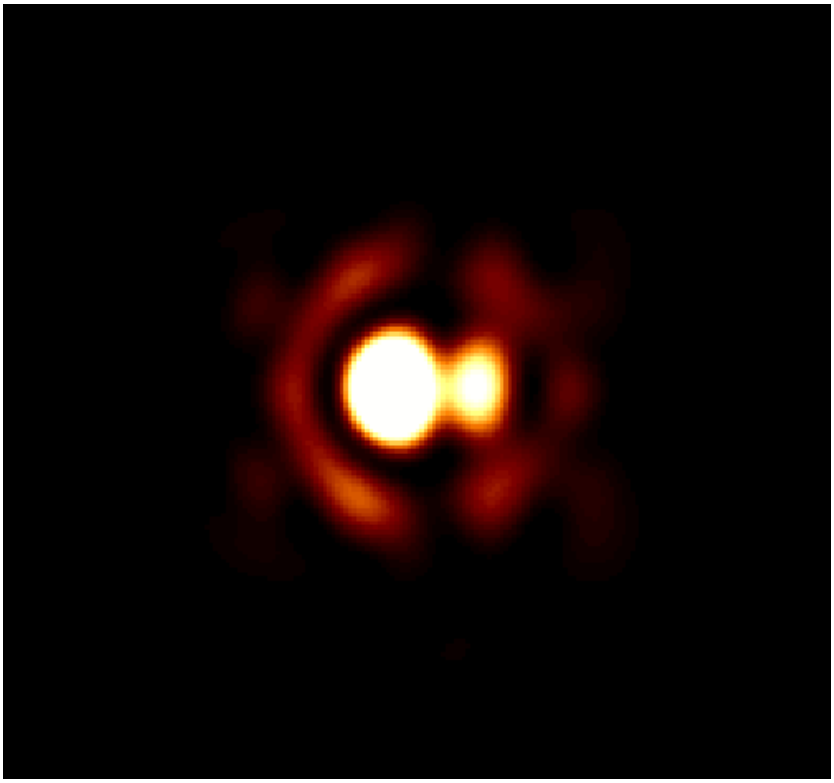

Figure 12: *Simulated PSF through a micro-mirror generated slits. The two-peaked shape of the PSF is the result of the phase shifts of the two mirrors in the center of the slit.*

where

$$k = 2\pi/\lambda \tag{13}$$

This expression suggests that it is not necessary to investigate spectrographs with a different origin of the WFE separately. However, it is not clear whether this applies to PSF generated by diffraction on MEMS arrays. Figure 13 compares the PSF for the case that all WFE were assigned to the telescope with the case when the *same* total WFE is distributed between telescope and spectrograph. It can be seen that the resulting PSF are noticeably different. For detailed investigation of the PSF in a MEMS spectrograph, the origin of the WFE has therefore to be taken into account.

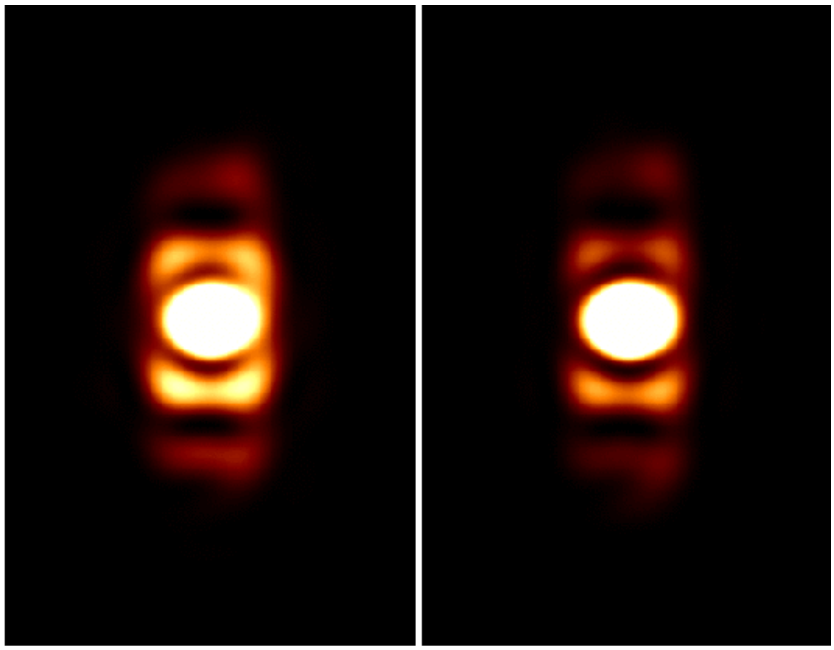

Figure 13: *Comparison of two monochromatic PSF resulting from telescope-spectrograph systems with a total WFE of 0.180μm. The left panel shows the PSF for the case that the WFE have been fully assigned to the telescope. The right hand panel shows the case where part of the same WFE is introduced by the spectrograph. Both panels have been plotted with the same colour scale.*

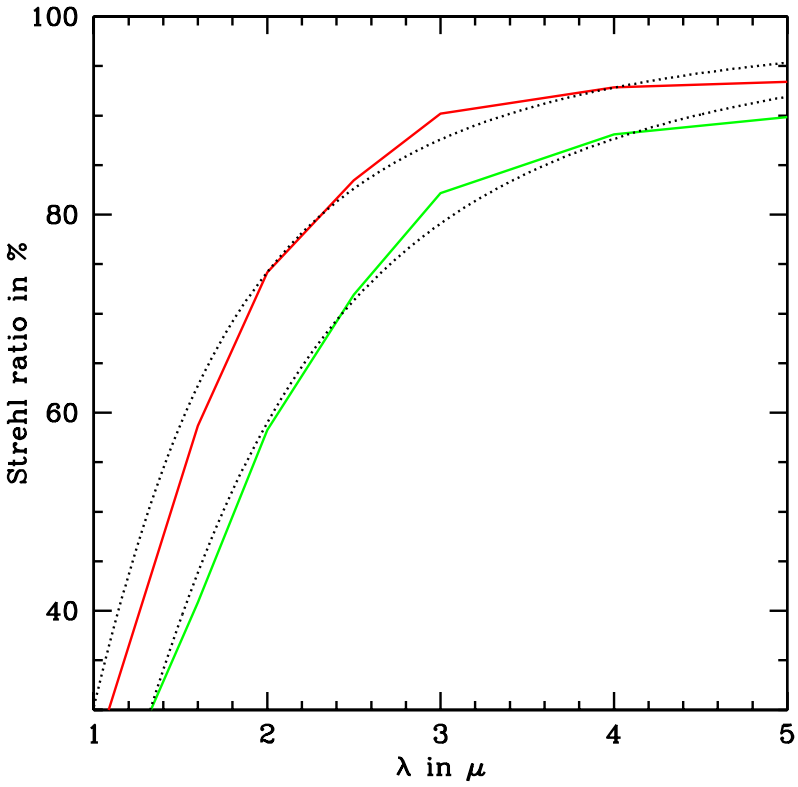

Figure 14: *Average Strehl ratio as a function of wavelength for a focused spectrograph. The WFE of the spectrograph was taken to be 0.088μm and 2 × 0.088μm for the red and green lines respectively . The dashed lines are the predicted Strehl ratios for near-perfect PSF with the same WFE.*

6.3 Average image quality

The actually achieved PSF and its Strehl ratio will be different for different positions within the slit. Here, we want to investigate how the image quality averaged over all dither positions compares to the near-perfect image quality which can be achieved by fully transparent slits. For that purpose, we have computed the Strehl ratios as a function of wavelengths for a grid of positions within the slit. WFE of the telescope can usually not be compensated by focusing the spectrograph since by construction focusing and other WFE are orthogonal to each other. However, since only some of WFE errors pass the MEMS generated slit, this

orthogonality gets lost. In this computation, we have used a focus position which maximizes the average Strehl ratio. The results for a spectrograph WFE of 0.88 and $2 \times 0.88\mu m$ are shown in figure 14. Also shown are the expected Strehl ratios for nearly perfect PSF of a telescope with the same total WFE. It can be seen that the *average* Strehl ratio over all positions within the slit is closely approximated by a nearly-perfect PSF.

7. Conclusion

Based on the analysis of a Fourier model of point-like objects, we find the following.

- ❏ The overall efficiency of a MEMS generated slit is typically on the order of 50 ± 10%. Typical exposure times are therefore on the order of at least 3 times the exposure time for an ideal slit. In order for a MEMS spectrograph to be more efficient than mechanical slit masks, the object density has to be such that the multiplexing of the MEMS slit is higher by this factor.
- ❏ The efficiency of NIRSpec cannot significantly be improved by increasing the collimator oversizing to more than about 20%.
- ❏ Mirrors are more efficient than shutters if their gap size is assumed to be half the one of the shutters. The phase errors introduced by the mirrors do not remove this efficiency advantage of the mirrors.
- ❏ However, the diffraction effects alone already reduce the achievable contrast ratio of mirrors close to the minimum acceptable level.
- ❏ For wavelengths longer than $3\mu m$, the efficiency of slits which are 3 facets wide strongly increases with wavelength. At the longest wavelengths, such a wider slit will therefore be of advantage for the most sensitive observations.
- ❏ Due to diffraction on the gaps between the facets, the image quality as measured by the Strehl ratio varies within the slit. For shutters, the average image quality is close to that of a near-perfect PSF with the same wavefront errors.
- ❏ Phase errors introduced by the facets will further reduce the image quality for micro-mirror arrays. The image quality of mirrors is lower than for the shutters even though smaller gaps were assumed.

Acknowledgments: This investigation of diffraction on MEMS generated slits is the results of numerous discussions with Peter Jakobsen. Bob Fosbury and Stefano Cristiani significantly contributed to this work through critical discussions. Thanks are also due to Bob also for the preparation of the final version of the text. Richard Hook proof-read an earlier draft of this work.

References

Freudling, W., Cristiani, S., Fosbury, R., Jakobsen, P., Pirzkal, N., 2002, ISR NGST 2002-03

Jakobsen, P., 2002, private communication

Krist, J., 2002, private communication

Schroeder, D., 1987, “Astronomical Optics”, Academic Press, Inc.